

RecNet: A Convolutional Network for Efficient Radiomap Reconstruction

Qun Niu¹, Ying Nie¹, Suining He², Ning Liu¹ and Xiaonan Luo^{3*}

¹Sun Yat-sen University

²The Hong Kong University of Science and Technology

³Guilin University of Electronic Technology

Email: ¹{niuqun@mail2,niey7@mail2,liuning2@mail}.sysu.edu.cn, ²sheaa@cse.ust.hk, ³luoxn@guet.edu.cn

Abstract—Wireless signals have been a strong indicator of nearby wireless environment, which can be used in a wide range of applications, including the construction and maintenance of wireless network in smart cities. However, wireless signals can change drastically due to moving pedestrians and automatic power adjustment of Access Points (APs), which renders previous radiomap inaccurate. To achieve sufficient accuracy, surveyors have to update the radiomap constantly, which incurs high maintenance cost in the long run.

To address this, we propose *RecNet*, a neural network to reconstruct a fine-grained radiomap with a small number of new samples. The intuition lies in the visualization of numerical signal strength values by a *heatmap*. A high-resolution heatmap corresponds to a fine-grained radiomap while a low-resolution one corresponds to a coarse-grained radiomap. Then we reduce the radiomap reconstruction to the image super-resolution: generating a high-resolution image from a low-resolution one. Based on the above, we design and implement the RecNet based on the image super-resolution neural network. Extensive experiments in two large test sites demonstrate that RecNet is able to reconstruct an accurate radiomap with only 50% of fingerprints, and reduces the signal error by more than 20% compared with a recent reconstruction algorithm.

I. INTRODUCTION

Smart cities aim at improving lives of citizens and boosting the economy with state-of-the-art technologies. Of all these, wireless signals (e.g., Wi-Fi, Bluetooth, Radio Frequency Identification) play a fundamental role as they are cornerstones of many high-layer applications, such as air quality monitoring, traffic control, anomaly detection, among others.

Wireless Received Signal Strength Indicator (RSSI), which often varies with positions and surroundings, provides valuable semantic clues about the wireless environment both indoors and outdoors. To evaluate this, researchers collect wireless fingerprints (a vector of RSSIs from different APs) and construct a corresponding radiomap (a set of fingerprints with location labels). Based on this map, they can determine the wireless status and provide timely services.

However, the radiomap may be outdated with time due to environmental changes, such as automatic power adjustment of APs [1], changing crowds of people and humidity levels [2]. In this case, the radiomap can change drastically, resulting

in erroneous environmental evaluation. To reduce these drawbacks, surveyors have to update the radiomap regularly, which is time-consuming and labor-intensive in large sites. Take our experiment in a building (covering 4,500 m^2) with 475 Reference Points (RPs) for example, it takes us around 90 seconds to collect 20 fingerprints at each RP. Thus the total time consumption of site survey in this area is around 11.9 hours ($475 \times 90 \div 3600$).

To reduce the cost of manual site survey, researchers have proposed different strategies to reconstruct the radiomap efficiently (constructing a new radiomap based on a few new fingerprints) [3], [4]. These strategies can be broadly divided into the following two categories: propagation model-based radiomap reconstruction [5], [6] and crowdsourcing-based fingerprint sampling [7], [8]. Model-based methods make assumptions of signal distributions, which may not hold in the constantly changing indoor environment. Some crowdsourcing-based methods, on the other hand, compare the recovered trajectory with indoor floor plan. Due to the noisy motion sensors, the recovered path may drift over time, resulting in inaccurate location labeling.

In this paper, we also consider given crowdsourced fingerprints for radiomap reconstruction, but from an image processing angle. The intuition is that as all fingerprints together form a heatmap, i.e., an image consisting of RSSIs corresponding to each AP at the site, reconstructing fingerprints can be considered as an image reconstruction. In other words, we model a sparse set of fingerprints, as namely a low-resolution “radiomap”, and augment it into a high-resolution one while reducing the labor-intensive survey cost. To realize image super-resolution, we adapt our RSSI reconstruction into a novel convolutional neural network. Figure 1 illustrates the reconstruction of AP D4:EE:07:49:76:EE in our test site, where each pixel represents an RP and the density value is the normalized sampled RSSI. We compare the granularity of heatmaps in this figure.

Specifically, we propose a Reconstruction Network, denoted as RecNet to reconstruct the radiomap efficiently. The key contributions of RecNet are as follows:

- Effective augmentation of heatmaps. With limited RPs in our test site, the number of pixels in the generated heatmaps is small, resulting in a lack of information.

*Corresponding author.

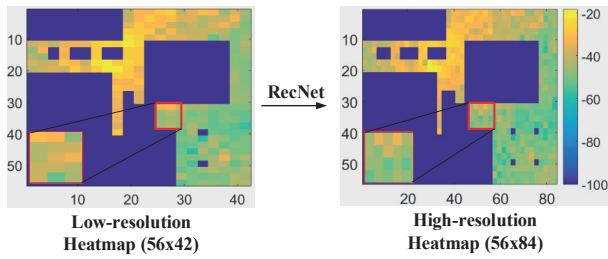


Fig. 1: Illustration of radio heatmap reconstruction. The aim of this work is to increase the heatmap granularity with low survey cost.

To address this, we propose an augmentation strategy by replicating rows and columns of heatmaps. Thus, we are able to increase the resolution of training heatmaps and improve the learned model. In addition to that, we also find that CNN is able to learn a better model with images in YCbCr space than RGB in our experiment. Therefore, we convert the fingerprints to YCbCr heatmaps.

- Patch-based learning of signal patterns. As discussed above, the signal distribution may suffer from local anomalies indoors, such as walls, ferromagnetic doors, among others. Instead of learning the holistic propagation model using the entire input heatmap, we crop it and train the neural network with cropped small overlapping patches. To achieve higher accuracy, we take the resolution of original heatmaps into the consideration and carefully select the patch size. By doing this, we are able to adapt the model locally and thus achieve higher accuracy.
- Experimental evaluations. To demonstrate the performance of the proposed system, we conduct two experiments in two large sites on our campus. Experimental results demonstrate that the proposed system is able to reduce the survey cost by 50% without compromising the accuracy.

Figure 2 illustrates the overall workflow of the radiomap reconstruction. For better viewing experiences, we generate a red bounding box for each low-resolution heatmap. In the offline stage, we first collect fingerprints at all RPs. Then, we extract the RSSI of a specific AP at each RP and build a heatmap. Afterwards, we downsample these heatmaps and generate a corresponding low-resolution counterpart for each original heatmap. (Refer to Section III for more details about heatmap downsampling.) We crop these heatmaps and feed the high/low-resolution pairs into the neural network. With the trained model, we are able to upscale the low input heatmap to a high-resolution one.

We have fully implemented the proposed RecNet and conducted experiments in two large test sites in our campus. Experimental results demonstrate that the proposed RecNet is able to reduce the reconstruction error by more than 20% compared with LDPL method with only a few samples (50%). Thus RecNet is able to facilitate the deployment of radio fingerprint-based systems in smart cities.

The remainder of this paper is structured as follows. We

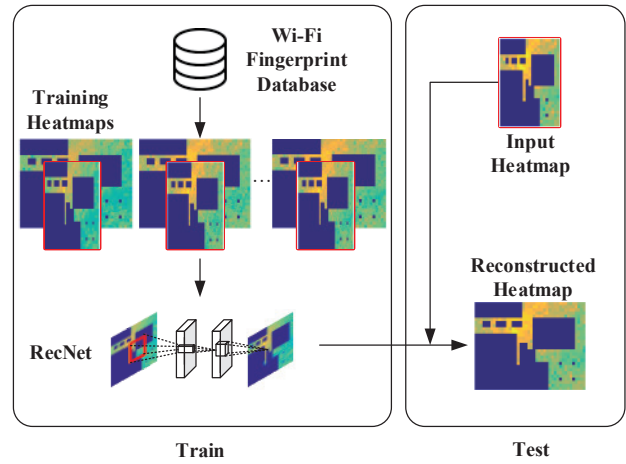


Fig. 2: The workflow of RecNet.

review the related work in Section II. Then we elaborate the design of radiomap reconstruction network in Section III. After presenting the experimental results in Section IV, we conclude the paper in Section V.

II. RELATED WORK

The pervasiveness of wireless devices enables a wide range of ubiquitous wireless sensing applications, such as localization [9], [10] and public transportation [11], to name a few. Although these applications have achieved sufficient accuracy, practical challenges, such as extensive cost of site survey and maintenance, hinder the deployment of such systems [12]. To address this, researchers have studied different methods to construct the radiomap effectively. These methods are divided into two categories: propagation model-based reconstruction and crowdsourcing-based radiomap reconstruction.

Log Distance Path Loss (LDPL) model [5] is employed to estimate the received signal strength based on the distance from the AP to the client. However, the accuracy may be compromised indoors with many wall partitions. Feng et al. [6] employ the sparsity of signals to facilitate signal reconstruction. Their method relies on the assumption that the signal is sparsely distributed indoors and satisfies the Gaussian distribution, which is not always feasible due to the dynamic nature of the indoor environment. Different from them, we do not rely on the pre-defined holistic signal propagation models. Instead, we crop patches from training heatmaps and *learn* the distribution of signals within these patches. Therefore, our method is location and environment-independent and achieves sufficient accuracy in the dynamically changing environment.

Crowdsourcing, on the other hand, provides another direction for efficient radiomap reconstruction. To reduce the survey cost, many works [13], [14] propose to employ the motion to assist the fingerprint collection. AcMu [7] employs the located static mobile devices to collect real-time fingerprints. By exploiting the underlying relationship of these fingerprints and their locations, they are able to update the radiomap accordingly. Apart from fusing Wi-Fi and motion, MPiLoc [8]

employs clustering algorithms to detect virtual landmarks (virtually prominent places with unique Wi-Fi, magnetic field or motion sensors patterns), such as lifts, stairs and so on to achieve higher accuracy. In summary, these methods reduce the cost of database construction and maintenance by offloading the survey to ordinary users. Different from them, the proposed method does not infer the user trajectories with noisy motion sensors. Thus it achieves higher stability.

Instead of using noisy motion sensors, some other methods propose to employ semi-supervised learning techniques with crowdsourced fingerprints, such as expectation maximization [15] and manifold-based learning [16], [17] in the radiomap reconstruction. More concretely, they first collect a small number of fingerprints with accurate location labels. Based on these labeled fingerprints, Chai et al. [15] and Shimosaka et al. [16] exploit the correlation between fingerprints in adjacent RPs and update the radiomap. These methods assume the signal correlation between physically nearby RPs, which can be easily disturbed by moving objects and walls. Different from them, our proposed RecNet does not make assumptions of the signal propagation or correlation between adjacent RPs. Instead, it crops patches from heatmaps and *learns* the patch-wise signal distribution through the state-of-the-art CNN. Therefore, it is robust in complicated scenarios. Moreover, it is also possible to employ the *transfer learning* to map the fingerprints collected by ordinary users to those at given positions. Thus our method can be easily integrated with current crowdsourcing-based reconstruction method to achieve efficient and accurate radiomap reconstruction.

Finally we discuss the single image super-resolution. State-of-the-art super-resolution CNN (SRCNN) [18] designs a neural network to learn an end-to-end mapping between the low-resolution and high-resolution exemplar image pairs. More recent super-resolution Generative Adversarial Network (SRGAN) [19] adds more layers to the network, which tends to generate *visually* attractive images rather than numerically accurate ones, which can result in a loss of reconstruction accuracy. Based on the above consideration, we consider adapting SRCNN in our task instead more recent neural networks.

III. NEURAL NETWORK DESIGN

In this section, we elaborate the process of reconstructing a high-resolution heatmap with a low-resolution one. We present preliminaries of image super-resolution in Section III-A. Then in Section III-B, we illustrate the visualization of numerical RSSI vectors sampled in our test site, followed by the architecture of RecNet in Section III-C.

A. Preliminaries of Image Super-Resolution

In the field of computer vision, image super-resolution is the process of recovering a high-resolution image from a low-resolution one. Previous example-based image SR usually consists of four main stages. First, the SR methods densely crop overlapping patches from the high-resolution images. Second, these methods learn a low-resolution dictionary and

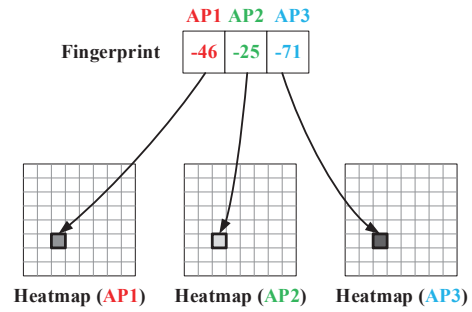


Fig. 3: An illustration of converting RSSI values to pixel values.

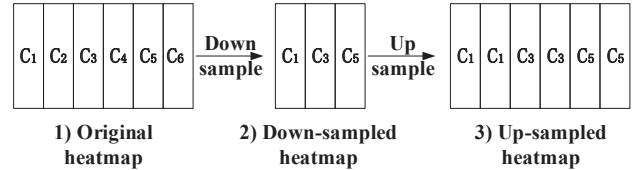


Fig. 4: The procedure of heatmap preparation.

encode these patches with it. Third, SR methods maps the low-resolution dictionary to a high-resolution dictionary and generate high-resolution patches. Lastly, SR jointly considers these reconstructed patches and recovers the high-resolution image with them. Interested readers can refer to [19] for more details.

B. Visualization of Radiomaps

Instead of numerical Wi-Fi fingerprints, conventional CNN processes RGB images. As a result, we visualize the discrete fingerprints in a test site and convert them into RGB images. Detailed visualization is presented as follows.

First we find the minimal and the maximal RSSI values of these fingerprints, denoted by $\underline{\psi}$ and $\hat{\psi}$, respectively. Then we map the RSSI values in the signal space to density values in the color space (ranging from 0 to 255). Given a numerical RSSI value ψ corresponding to an AP, we convert it to the density value as follows:

$$i = \left\lfloor \frac{\psi - \underline{\psi}}{\hat{\psi} - \underline{\psi}} * 255 \right\rfloor. \quad (1)$$

Based on Equation (1), we are able to convert all RSSI values to density values. Afterwards, we extract density values corresponding to the same AP and put them in the corresponding pixel location. Figure 3 illustrates the visualization process. Suppose we have a fingerprint with three APs sampled at RP z . First we convert these RSSIs to density values, then we put them at the corresponding image position in the heatmap. With fingerprints collected from all RPs, we create a heatmap for each AP. In some cases where some RPs are not accessible or some APs are not detected, we set the corresponding density values to zero.

We first conduct a comprehensive site survey and generate a high-resolution heatmap. Then, we downsample this high-resolution heatmap by removing every other column. Please

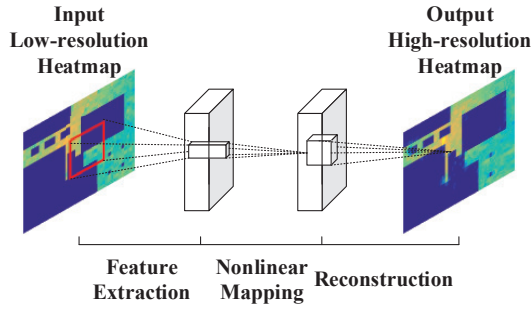


Fig. 5: The architecture of RecNet.

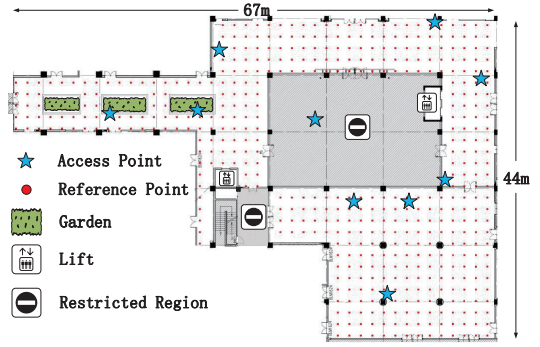


Fig. 6: The floor plan of SEIT..

note that it is also possible to conduct different downsampling strategies such as removing every other row. As we focus on exploiting the SR to radiomap reconstruction, we do not specifically compare different downsampling methods in this paper. As SRCNN requires that the high-resolution heatmap is the same size as the low-resolution one, we duplicate every column of the low-resolution heatmap (Figure 4). By doing so, we are able to generate a high and low-resolution heatmap pair. Then we replicate the density and fill the RGB channel with the same value to generate an RGB heatmap.

C. Structure of the Neural Network

In this section, we present the structure of RecNet. It is a 3-layer network (Figure 5) adopted from SRCNN [18].

The network has three convolutional layers. With the input of the low-resolution heatmap K (the corresponding high-resolution heatmap is denoted as X), the first convolutional layer contains a 9×9 filter. This layer convolves the input image with it. Mathematically, the convolution operation can be defined as follows:

$$Q_1 = \max(0, W_1 * K + B_1), \quad (2)$$

where W_1 is the filter and B_1 is the bias in this operation. The convolutional operator is denoted as $*$.

The second convolutional layer has a 1×1 filter. As explained in [18], the second operation is non-linear mapping of feature vectors generated in the first layer, which is equivalent to convolving with a 1×1 filter. Similarly, the operation in this layer is defined as follows:

$$Q_2 = \max(0, W_2 * Q_1 + B_2), \quad (3)$$

where W_2 and B_2 are corresponding filter and bias in this layer, respectively.

Finally, the third layer has a 5×5 filter. This layer *averages* the patches generated in the previous layer and outputs the high-resolution heatmap, denoted by X' . The operation in this layer is defined as follows:

$$X' = W_3 * Q_2 + B_3, \quad (4)$$

where W_3 and B_3 are corresponding filter and bias in this layer.

These filters are used in the convolution operations to process a patch of RSSI values. With larger filters, we are

able to take more RPs in the vicinity into consideration. The filter size of the last layer is smaller than that of the first layer because we put more emphasis on the central part of those high-resolution patches. However, if the size of a filter is too large, more faraway RPs are taken into consideration, which can degrade the accuracy with partitions. Therefore, we need to set the filter size accordingly to achieve trade-off between the number of RPs and the nearby obstructions.

Given an ground truth high-resolution heatmap X corresponding to the input heatmap K and the reconstructed high-resolution heatmap X' , we define the loss function using the mean squared error (MSE):

$$L = \|X - X'\|^2. \quad (5)$$

After preprocessing, we feed the high and low-resolution heatmap pairs into the RecNet and conduct the training. Please refer to Section IV for more details about the parameters of the network and our training configurations.

IV. EXPERIMENTAL RESULTS

We first discuss the experimental settings of the RecNet in Section IV-A. Then we present our dataset in Section IV-B, followed by the evaluations of reconstruction accuracy (Section IV-C) and localization results using reconstructed radiomap (Section IV-D).

A. Experimental Settings and Comparison Schemes

We evaluate our RecNet in the School of Electronics and Information (SEIT) and School of Super Computing (SC) in our campus. Figure 6 illustrates the test area (covering around $3,000 m^2$) in the first floor of SEIT while Figure 7 illustrates the floor plan (covering around $2,800 m^2$) in the fifth floor of SC. The configuration of SC differs from SEIT significantly. SEIT has large open space, while SC has many partitions with long narrow corridors.

The number of RPs in SEIT is 475 (1.6m grid size) while that in SC is 560 (1.2m grid size). In the course of the site survey, we collect 20 samples at each RP and store them along with their locations in a database. We generate the heatmaps of SEIT on June 18, 2017 and train the proposed RecNet for SEIT with these heatmaps. As for SC, we train our model with data collected on August 9, 2017. To test the reconstruction

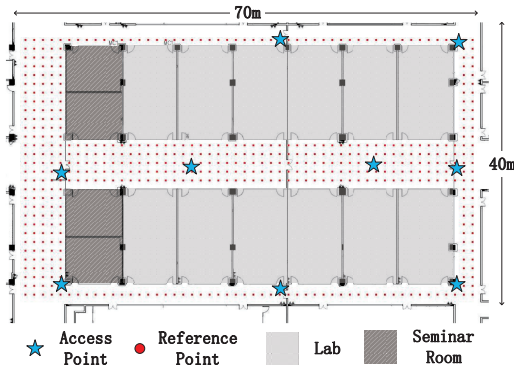


Fig. 7: The floor plan of SC.

accuracy, we conduct another site survey with the same grid size on July 22, 2017 in SEIT and September 10, 2017 in SC.

In our experiment, we evaluate the reconstruction accuracy using the following metric: the differences between recovered RSSI values and the ground truth ones. More specifically, we define the metrics as follows. Suppose we have M APs and N RPs in our test site, the differences between the recovered RSSI values and the ground truth ones are defined as follows:

$$\sum_{m=1}^M \sum_{n=1}^N |\phi_{mn} - \hat{\phi}_{mn}|, \quad (6)$$

where ϕ_{mn} denotes the reconstructed RSSI value of AP m ($1 \leq m \leq M$) at RP n ($1 \leq n \leq N$) and $\hat{\phi}_{mn}$ denotes the corresponding ground truth RSSI value.

We also integrate the recovered radiomap with the indoor localization algorithm [5] to evaluate the reconstruction accuracy. The differences between location estimations and ground truth ones are defined as follows:

$$\sum_{n=1}^N \|\mathbf{x}_n - \hat{\mathbf{x}}_n\|, \quad (7)$$

where N is the number of test locations, $\|\mathbf{x}_n - \hat{\mathbf{x}}_n\|$ is the Euclidean distance between the estimated location \mathbf{x}_n and the ground truth $\hat{\mathbf{x}}_n$.

We compare RecNet with the *LDPL* [5], which recovers the RSSI at an RP based on its distance to an AP. We implement this scheme and recover the radiomap based on APs with known locations using this model.

B. Our Dataset

In this section, we detail the generation of our dataset. After collecting 20 samples at each RP, we extract RSSI values corresponding to each AP in the whole test site and convert them to density values. As we cannot conduct site survey in restricted areas such offices and conference rooms, we manually set the RSSI values of RPs in these regions to the lowest RSSI value.

In summary, we generate 20 heatmaps for each AP, 15 of which are used for network training, 4 are used for validation. Then we crop overlapping patches from the training heatmaps with specified sizes (21×21) with step length 2. Finally, we

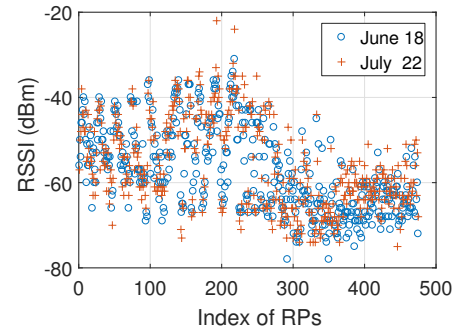


Fig. 8: Comparison of RSSIs for one AP (SEIT).

are able to generate around 15,000 patches for each AP, which is sufficient for our training. In our experiment, we find that larger resolution of heatmaps often leads to higher reconstruction accuracy. Therefore, we manually augment the samples by duplicating columns of heatmaps.

C. Reconstruction Accuracy

In this section, we present the reconstruction accuracy and the impact of training iterations on it.

Figure 8 illustrates the ground truth RSSI values for AP D4:EE:07:49:76:EE in our test site. In this figure, blue circles represent the RSSI values collected on June 18, while the red pluses represent the values on July 22. Experimental results in this test site show that the average RSSI differences of these RPs on different dates is around 5.083dB, which is significant in this period.

Figure 9 shows the reconstruction accuracy of RecNet. From this figure, we can learn that the reconstruction accuracy of RecNet is higher than LDPL. The reasons are as follows. LDPL models the signal with holistic propagation pattern. However, it does not work well indoors with many wall partitions and moving pedestrians. Different from LDPL, RecNet learns the distribution of signals from small overlapping patches of the original heatmaps. Consequently, it can adjust to local anomalies, such as wall partitions and occlusions. In addition to that, RecNet is able to achieve higher accuracy due to the bidirectional propagation during the training, which can give feedback on the training results. Based on the above reasons, RecNet provides better estimation accuracy.

Figure 10 compares the reconstruction accuracy of RecNet and LDPL in SC. It demonstrates that our RecNet achieves higher accuracy in this test site. LDPL achieves insufficient accuracy because the multipath propagation, as well as the surrounding walls render holistic log distance model inapplicable. In contrast to LDPL, RecNet learns the signal distribution locally from small patches, thus it is able to achieve higher accuracy in this complicated test site.

Figure 11 presents the mean RSSI differences with different numbers of iterations during training. It shows that the reconstruction error first decreases. This is because with more iterations, the trained network is able to fit our training data. With more than 200,000 iterations, the network may overfit the training data, thus the test error begins to increase. As a

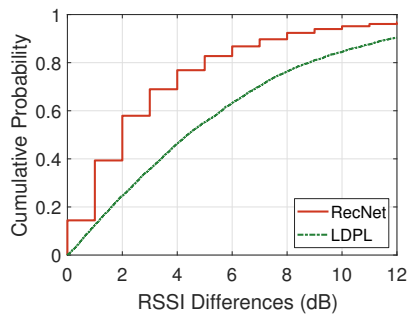


Fig. 9: CDF of RSSI difference (SEIT).

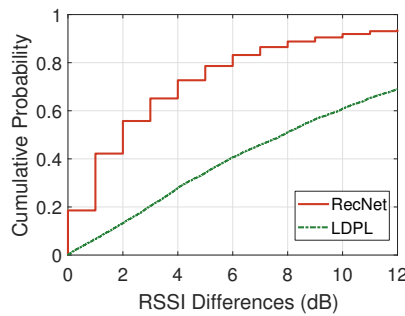


Fig. 10: CDF of RSSI difference (SC).

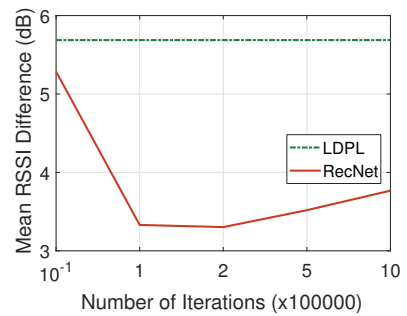


Fig. 11: Mean RSSI difference v.s. number of iterations during training (SEIT).

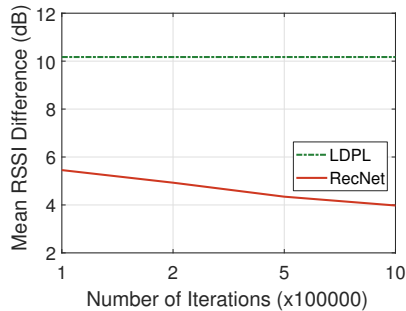


Fig. 12: Mean RSSI difference v.s. number of iterations during training (SC).

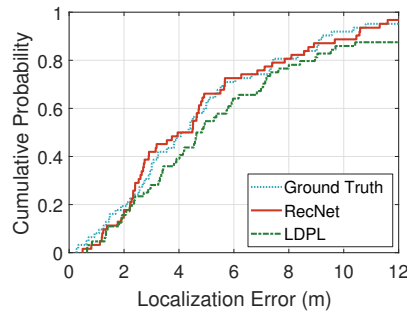


Fig. 13: CDF of localization error on the first floor in SEIT.

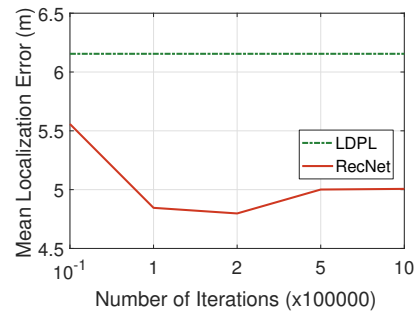


Fig. 14: Mean localization error v.s. number of iterations (SEIT).

result, the number of iterations in the training stage is set to 100,000 in our experiment to achieve trade-off between the reconstruction accuracy and time consumption of training.

Figure 12 shows the mean RSSI differences with the number of training iterations in SC. It shows that our RecNet outperforms LDPL. Compared with that in SEIT, the reconstruction accuracy is higher in SC due to the following reason. The configuration of SC is significantly different from that in SEIT. For example, the SEIT has much open space in the entrance hall. In contrast, SC has many long narrow corridors, which incur serious multipath effect. Thus the line-of-sight-based LDPL does not achieve sufficient accuracy. Different from LDPL, RecNet does not make assumptions of the environment or the holistic signal propagation model. Instead, it learns the signal pattern with local patches. Thus it is able to deal with local anomalies and achieve higher accuracy.

D. Comparison of Localization Error

In this section, we evaluate the localization error with the reconstructed heatmaps.

Figure 13 shows the localization error with reconstructed radiomaps in SEIT. It shows that CDF of the localization error reduces by than 20% with our reconstructed map and achieve comparable accuracy with manual site survey. This demonstrates that our proposed RecNet is able to adapt to the environment effectively. Therefore, the localization system is also able to achieve stable localization accuracy in the dynamically changing environment.

Figure 14 shows the mean localization error with the number of iterations during the training stage. It shows that the

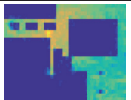
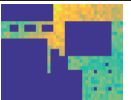
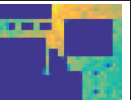
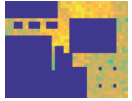
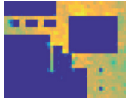
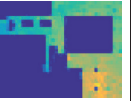
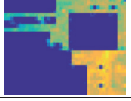
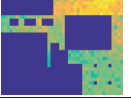
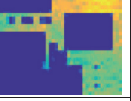
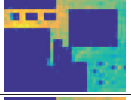
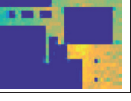
localization first decreases with more iterations. It is because that the RecNet is able to adapt to the training data with more iterations. Thus the reconstruction accuracy increases at first, leading to lower localization error. However, when the number of iteration is sufficiently large (i.e., 200,000), the localization error begins to increase. This is because the RecNet overfits the existing training data and achieves lower reconstruction accuracy with new data.

Table I presents the illustrative reconstructed heatmaps with 100,000 iterations. We can see from these images that the reconstructed heatmaps are similar to the ground truth ones. The quantitative mean RSSI difference also demonstrates that the RecNet is able to achieve sufficient reconstruction accuracy. Of all the APs, RecNet achieves the lowest accuracy on AP D4:EE:07:4A:CA:1A (mean RSSI difference 4.44 dB). This is because AP D4:EE:07:4A:CA:1A is close to walls and nearby pieces of furniture such as tables, which can incur stronger multi-path effect, thus increasing the reconstruction error.

V. CONCLUSION

Ubiquitous wireless signals have been playing an important role in a wide range of applications. However, due to environmental fluctuations, previously collected radiomap often changes dramatically over a long time, which incurs constant overhead of maintenance. To address this, we propose RecNet, a convolutional neural network for efficient and effective radiomap reconstruction. To achieve sufficient accuracy, RecNet maps the RSSI to pixel values. Based on these converted values and corresponding locations, it generates heatmaps for

TABLE I: Illustrative reconstruction of heatmaps in SEIT.

AP	Mean RSSI Difference	Ground Truth	RecNet	AP	Mean RSSI Difference	Ground Truth	RecNet
AP1	3.34dB			AP6	3.14dB		
AP2	3.05dB			AP7	3.47dB		
AP3	4.44dB			AP8	3.36dB		
AP4	3.19dB			AP9	3.39dB		
AP5	2.99dB			AP10	2.92dB		

each AP. To facilitate effective training, RecNet augments heatmaps to enhance the training accuracy. It addresses local signal fluctuations by employing a patch-wise learning paradigm. Therefore, it loosens the requirement of indoor configurations and is more robust to local signal anomalies. Experimental results in two different test sites demonstrate that RecNet is able to reconstruct an accurate radiomap after a month with sufficient accuracy using only 50% fingerprints.

ACKNOWLEDGMENT

This work was supported, in part, by National Natural Science Foundation of China under Grant 61472455,61320106008 and Guangzhou Science Technology and Innovation Commission (GZSTI16EG14/201704030079).

REFERENCES

- [1] S. He, W. Lin, and S.-H. G. Chan, "Indoor localization and automatic fingerprint update with altered ap signals," *IEEE Transactions on Mobile Computing*, vol. 16, no. 7, pp. 1897–1910, July 2017.
- [2] Y.-C. Chen, J.-R. Chiang, H.-h. Chu, P. Huang, and A. W. Tsui, "Sensor-assisted Wi-Fi indoor location system for adapting to environmental dynamics," in *Proc. ACM MSWiM*. ACM, 2005, pp. 118–125.
- [3] B. Yang, S. He, and S.-H. G. Chan, "Updating wireless signal map with bayesian compressive sensing," in *Proc. ACM MSWiM*, 2016, pp. 310–317.
- [4] S. He and S. H. G. Chan, "Towards crowdsourced signal map construction via implicit interaction of iot devices," in *Proc. IEEE SECON*, June 2017.
- [5] P. Bahl and V. N. Padmanabhan, "RADAR: An in-building RF-based user location and tracking system," in *Proc. IEEE INFOCOM*, March 2000, pp. 775–784.
- [6] C. Feng, W. S. A. Au, S. Valaee, and Z. Tan, "Received-signal-strength-based indoor positioning using compressive sensing," *IEEE Transactions on Mobile Computing*, vol. 11, no. 12, pp. 1983–1993, Dec 2012.
- [7] C. Wu, Z. Yang, and C. Xiao, "Automatic radio map adaptation for indoor localization using smartphones," *IEEE Transactions on Mobile Computing*, to appear.
- [8] C. Luo, H. Hong, M. C. Chan, J. Li, X. Zhang, and M. Zhong, "MPiLoc: Self-calibrating multi-floor indoor localization exploiting participatory sensing," *IEEE Transactions on Mobile Computing*, vol. 17, no. 1, pp. 141–154, Jan 2018.
- [9] S. He, S. H. G. Chan, L. Yu, and N. Liu, "Fusing noisy fingerprints with distance bounds for indoor localization," in *Proc. IEEE INFOCOM*, April 2015, pp. 2506–2514.
- [10] J. Wang, N. Tan, J. Luo, and S. J. Pan, "WOLoc : Wifi-only outdoor localization using crowdsensed hotspot labels," in *Proc. INFOCOM*. IEEE, 2017, pp. 1–9.
- [11] R. Verma, A. Shrivastava, B. Mitra, S. Saha, N. Ganguly, S. Nandi, and S. Chakraborty, "UrbanEye: An outdoor localization system for public transport," in *Proc. IEEE INFOCOM*. IEEE, 2016, pp. 1–9.
- [12] S. He and S.-H. G. Chan, "Wi-Fi fingerprint-based indoor positioning: Recent advances and comparisons," *IEEE Communications Surveys & Tutorials*, vol. 18, no. 1, pp. 466–490, 2016.
- [13] L. Xiang, T. Y. Tai, B. Li, and B. Li, "*Tack*: Learning towards contextual and ephemeral indoor localization with crowdsourcing," *IEEE Journal on Selected Areas in Communications*, vol. 35, no. 4, pp. 863–879, April 2017.
- [14] Z. Yin, C. Wu, Z. Yang, and Y. Liu, "Peer-to-peer indoor navigation using smartphones," *IEEE Journal on Selected Areas in Communications*, vol. 35, no. 5, pp. 1141–1153, May 2017.
- [15] X. Chai and Q. Yang, "Reducing the calibration effort for probabilistic indoor location estimation," *IEEE Transactions on Mobile Computing*, vol. 6, no. 6, pp. 649–662, June 2007.
- [16] M. Shimosaka and O. Saisho, "Efficient calibration for RSSI-based indoor localization by bayesian experimental design on multi-task classification," in *Proc. ACM UbiComp*. ACM, 2016, pp. 244–249.
- [17] K. Majeed, S. Sorour, T. Y. Al-Naffouri, and S. Valaee, "Indoor localization and radio map estimation using unsupervised manifold alignment with geometry perturbation," *IEEE Transactions on Mobile Computing*, vol. 15, no. 11, pp. 2794–2808, Nov 2016.
- [18] C. Dong, C. C. Loy, K. He, and X. Tang, "Image super-resolution using deep convolutional networks," *IEEE Transactions on Pattern Analysis and Machine Intelligence*, vol. 38, no. 2, pp. 295–307, Feb 2016.
- [19] C. Ledig, L. Theis, F. Huszar, J. Caballero, A. Cunningham, A. Acosta, A. Aitken, A. Tejani, J. Totz, Z. Wang, and W. Shi, "Photo-realistic single image super-resolution using a generative adversarial network," in *Proc. IEEE CVPR*, July 2017.